

1 **Supplemental Materials**

2

3 Danicamtiv reduces myosin's working stroke but enhances contraction by activating the

4 thin filament

5

6 Brent Scott, Lina Greenberg, Caterina Squarci, Kenneth S. Campbell, and Michael J.

7 Greenberg

## 8 **Supplemental Methods**

9

### 10 **Proteins and Solutions**

11 Full length  $\beta$ -cardiac myosin and actin were purified from porcine left ventricular  
12 tissue as we have previously done (1). The proteolytic cleavage of full-length myosin into  
13 myosin sub-fragment 1 (S1) by chymotrypsin was performed as described by previously  
14 described (2, 3). Actin was prepared from acetone powder as previously described (4).  
15 Actin was labeled with n-(1-pyrene)iodoacetamide for stopped flow experiments as  
16 previously described (5). All actin was phalloidin stabilized in a 1.1:1 ratio. Human  
17 troponin and tropomyosin were expressed in *E. coli* and purified as previously described  
18 (2). All experiments were performed in KMg25 buffer unless otherwise noted (25 mM KCl,  
19 10 mM EGTA, 60 mM MOPS pH 7.0, 1 mM DTT, and 5 mM  $MgCl_2$ ). Danicamtiv was  
20 purchased from Selleckchem and dissolved in DMSO (99.1% purity, S9948) and diluted  
21 in KMg25 to a final concentration of 10  $\mu$ M in the final assay buffers. The experiments  
22 were conducted with 0.1% DMSO controls.

23

### 24 **Steady-State ATPase Measurements**

25 The steady-state ATPase rate of myosin was measured using the NADH-linked  
26 assay as we have previously done (6-8). The NADH-linked ATPase measurements were  
27 conducted with myosin S1 in a specific ATPase buffer containing 20 mM Imidazole pH  
28 7.5, 10 mM KCl, 2 mM  $MgCl_2$ , and 1 mM DTT assayed in a BioTek Synergy H1M plate  
29 reader using a 96 well plate with shaking at 25°C. Absorbance was monitored at 340 nm  
30 continuously over 10 minutes. The contribution of actin alone to the ATPase rate was

31 subtracted. Data showing the rate as a function of actin concentration were fitted using  
32 the Michaelis-Menten equation.

33

### 34 **Stopped Flow Transient Kinetics**

35 Stopped flow measurements were conducted in an SX-20 instrument from Applied  
36 Photophysics. All nucleotide concentrations were determined spectroscopically. All  
37 stopped flow assays used myosin S1. Experiments were conducted in KMg25 at 20°C.  
38 For the measurements of ATP-induced dissociation, ADP release, ADP affinity, and single  
39 turnovers, pyrene-labeled actin was used with an excitation wavelength of 365 nm and a  
40 395 nm filter before the photomultiplier tube. Measurement of ATP hydrolysis was done  
41 using intrinsic tryptophan fluorescence, with an excitation wavelength of 295 nm and a  
42 320 nm filter placed before the photomultiplier tube. All concentrations are given before  
43 mixing.

44 We measured the rate of ADP release from actomyosin  $k_{+5}$  as we have previously  
45 done (1, 2, 5, 9). Briefly, 1  $\mu\text{M}$  myosin, 1  $\mu\text{M}$  pyrene actin, and 100  $\mu\text{M}$  Mg.ADP were pre-  
46 incubated in syringe 1 and rapidly mixed 5000  $\mu\text{M}$  Mg.ATP. Resultant fluorescence  
47 transients were well fitted by a single exponential function to provide the rate of ADP  
48 release.

49 To measure the ADP affinity,  $K_5'$ , we pre-incubated 1  $\mu\text{M}$  myosin, 1  $\mu\text{M}$  pyrene  
50 actin, and a variable amount of Mg.ADP. We then rapidly mixed this with 100  $\mu\text{M}$  Mg.ATP.  
51 Fluorescence transients were well fitted by single exponential functions. The observed  
52 rate was plotted as a function of ADP, and the resultant curve was well fitted by a  
53 hyperbolic curve:

54

$$k_{obs} = \frac{k_0}{1 + \frac{[ADP]}{K_5'}}$$

55 where  $k_0$  is the rate in the absence of ADP and  $K_5$  is the ADP affinity. From the measured  
56 rate of ADP release and the ADP affinity, it was possible to calculate the rate of ATP  
57 binding to actomyosin,  $k_{-5}$ .

58 The rate of ATP-induced actomyosin dissociation was measured as we have  
59 previously done (1, 2, 5, 9). 1  $\mu$ M myosin, 1  $\mu$ M pyrene actin, and 0.04 U/mL apyrase VII  
60 were pre-incubated in syringe 1 and then rapidly mixed varying concentrations of Mg.ATP.  
61 Fluorescence transients were well fitted by the sum of two exponential functions, as  
62 previously described (6). The fast phase reports the rate of ATP binding and subsequent  
63 actomyosin dissociation. The slow phase reports on a well-established nucleotide  
64 isomerization. The amplitude of the fast phase was fixed at low ATP concentrations  
65 because some signal is lost in the dead time at higher concentrations of ATP. The  
66 observed rate of the fast phase increases hyperbolically with ATP concentration, and the  
67 data was fitted with the hyperbolic function:

68

$$k_{fast} = \frac{k_{+2}'[ATP]}{K_1' + [ATP]}$$

69 The observed rate of the slow phase at saturating ATP concentrations reports the rate of  
70 the nucleotide isomerization  $k_{+\alpha}$ . The ratio of the fast and slow amplitudes can be used to  
71 calculate the equilibrium constant for the nucleotide free isomerization,  $K_\alpha$ . The reverse  
72 rate constant can be calculated from the forward rate and the equilibrium constant.

73 To measure the rate of ATP binding and hydrolysis to myosin, we used the intrinsic  
74 tryptophan fluorescence of myosin that changes with hydrolysis (6). We preincubated 2  
75  $\mu$ M myosin with 0.04 U/mL apyrase VII and then rapidly mixed this with a range of ATP

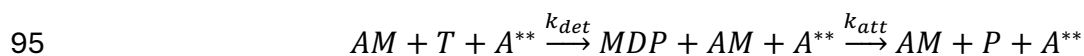
76 concentrations. The individual fluorescence transients were well fitted by single  
77 exponential functions, and the relationship between the observed rate and the ATP  
78 concentration was well fitted by a hyperbolic function.

79

## 80 **Single Turnover Measurements of Actomyosin Detachment and Attachment**

81 To measure the rates of actomyosin detachment ( $k_{det}$ ) and attachment at a given  
82 concentration of actin ( $k_{att}$ ), we used a single turnover measurement (10). For practical  
83 experimental reasons, this experiment could not be performed under optimal pseudo-first  
84 order conditions. As such, the data show some deviation from single exponential  
85 behavior, and it is more appropriate to solve the system of differential equations. We  
86 mixed 2.5  $\mu$ M myosin and 10  $\mu$ M pyrene labeled actin (all concentrations after mixing) to  
87 form 2.5  $\mu$ M actomyosin (AM) and 7.5  $\mu$ M free pyrene actin ( $A^{**}$  where the stars denote  
88 fluorescence). We monitored the change in pyrene fluorescence since free pyrene actin  
89 has high fluorescence while myosin bound to pyrene actin has quenched fluorescence.  
90 We then rapidly added 0.75  $\mu$ M ATP (T). ATP binding to actomyosin causes rapid  
91 detachment of the myosin, which can be seen by an increase in fluorescence. Then ATP  
92 bound to myosin undergoes rapid hydrolysis to myosin\*ADP\*Pi (MDP). MDP can then  
93 reattach to the actin, quenching the fluorescence and releasing phosphate (P).

94 Data were analyzed with the following overall kinetic scheme:



96 The reaction followed the set of differential equations:

$$97 \quad \frac{d[AM]}{dt} = -k_{det}[AM] * [T] + k_{att}[A^{**}] * [MDP]$$

98 
$$\frac{d[A^{**}]}{dt} = k_{det}[AM] * [T] - k_{att}[A^{**}] * [MDP]$$

99 
$$\frac{d[T]}{dt} = -k_{det}[AM] * [T]$$

100 
$$\frac{d[MDP]}{dt} = k_{det}[AM] * [T] - k_{att}[A^{**}] * [MDP]$$

101 
$$\frac{d[P]}{dt} = k_{att}[A^{**}] * [MDP]$$

102 The initial starting conditions were [AM] = 2.5 μM, [T] = 0.75 μM, [A] = 7.5 μM, [MDP] = 0,  
103 and [P] = 0. In the stopped flow, we observe the change in the fluorescence as MDP is  
104 formed and then disappears, so our measured fluorescence signal is proportional to the  
105 [MDP]. The normalization constant of this signal was a fitting parameter.

106 These experiments could not be performed under pseudo-first order conditions,  
107 and therefore data needed to be analyzed by solving a set of differential equations. We  
108 used the ode45 function in Matlab and least squares optimization to solve the system of  
109 differential equations for the values of  $k_{att}$  and  $k_{det}$  that best fit the experimental data (as  
110 well as the normalization constant to convert fluorescence signal to concentration)  
111 **(Supplemental Figures 3 and 4).**

112 Consistent with our transient kinetic and optical trapping experiments, the single  
113 turnover transients demonstrate that 10 μM danicamtiv does not change detachment  
114 kinetics **(Supplemental Fig. 4C)**. Moreover, these experiments demonstrate that 10 μM  
115 danicamtiv increases the attachment kinetics **(Supplemental Fig. 4D)**. It is important to  
116 note that these measurements could not be conducted at saturating concentrations of  
117 actin due to experimental limitations. As such, the rate of attachment here does not  
118 represent the maximal rate of attachment; however, our transient and steady-state kinetic

119 experiments demonstrate that the overall ATPase cycle is not limited by detachment  
120 kinetics. The steady-state ATPase experiments clearly demonstrate that danicamtiv  
121 increases the ATPase rate, likely through effects on attachment kinetics.

122

### 123 ***In vitro* Motility Assays**

124 *In vitro* motility assays were performed as previously described (1, 2, 5, 9). For  
125 regulated motility, thin-filaments were reconstituted by the addition of 0.5  $\mu$ M troponin and  
126 0.5  $\mu$ M tropomyosin. For the regulated motility experiments, the levels of free calcium  
127 were set using MaxChelator (11). Videos were recorded at room temperature and  
128 analyzed using MTrackJ (12) in Fiji (13).

129

### 130 **Optical Trapping**

131 All optical trapping assays were conducted on a custom-built microscope free  
132 setup as described previously (1, 14, 15). Full length myosin underwent a deadhead spin  
133 down on the day of experimentation, and it was diluted to achieve single molecule  
134 conditions (1-3 nM). The final assay buffer was KMg25 with 1 mg/mL BSA, the desired  
135 ATP concentration, 5-10 nM TRITC biotin F-actin, 1 mg/mL glucose, 192 U/mL glucose  
136 oxidase, and 48  $\mu$ g/mL catalase. Experiments were performed at room temperature.

137 The analysis of optical trapping data was performed using automated event  
138 detection based on changes in the covariance between the optically trapped beads (14).  
139 For the 1 mM ATP trapping dataset, analysis was done using a separate software program  
140 (16) that is available as an R package and is available on GitHub  
141 (<https://github.com/brentscott93/lasertrapr>). At 1 mM ATP, myosin's rigor lifetime is very

142 short lived (~1 ms) making it impossible to resolve substeps of the myosin working stroke.  
143 For the 1 mM ATP dataset, the total displacement is measured from the average position  
144 across the duration of the binding event. For all datasets, the cumulative distributions  
145 were using with maximum likelihood estimation as described previously (17).

146 For the load-dependent measurements of actomyosin interactions, experiments  
147 were conducted at saturating (1 mM) ATP. Data were analyzed by applying a Hidden  
148 Markov model and changepoint analysis to the position of the motor bead. The average  
149 force was calculated across the duration of the binding event. Data were fitted to the Bell  
150 equation using maximum likelihood estimation and confidence intervals were calculated  
151 by bootstrapping simulations (17).

152

### 153 **Computational modelling with FiberSim**

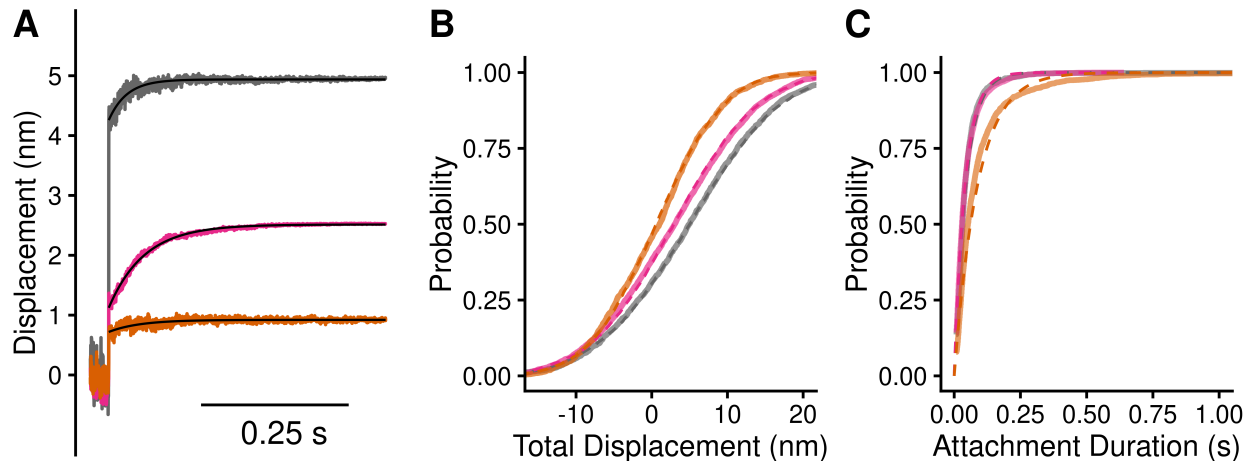
154 To simulate the molecular effects of danicamtiv in muscle, we used FiberSim (18).  
155 FiberSim is a spatially explicit model of muscle contraction based on fundamental  
156 biophysical properties. We used a previously validated base model to serve as a  
157 reference control. To model the molecular effects of danicamtiv, we changed three  
158 parameters in the model (1) the myosin step size, (2) the population of active myosin  
159 heads, and (3) the attachment rate. We examined the effects of changing these  
160 parameters both in isolation and in combination. All the configuration and relevant model  
161 files are in the project repository hosted on Zenodo. FiberSim 2.1.0 was used to run the  
162 simulations on a Windows 10 computer.

163

### 164 **Statistical Analysis**

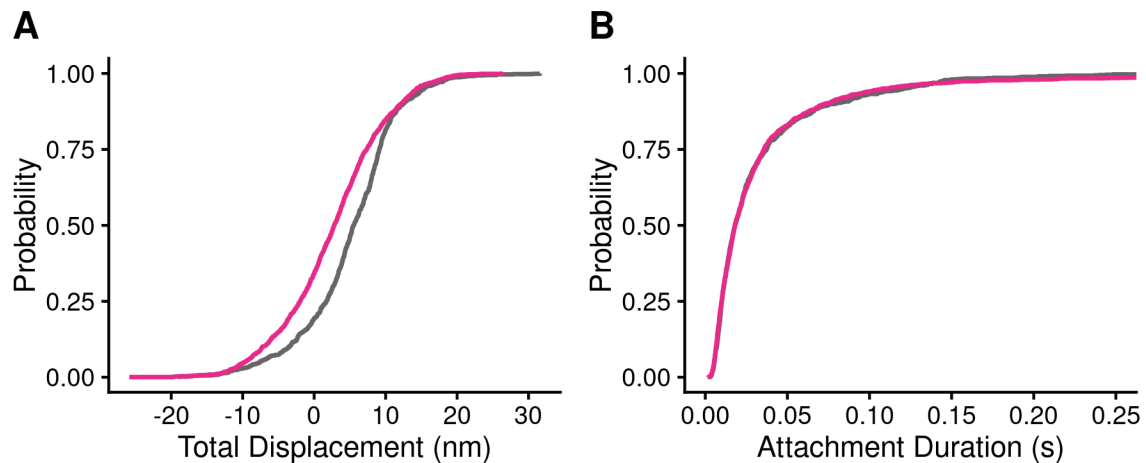


165 All data was collected over multiple days from at least 2 independent protein preparations.  
166 For the ATPase, stopped flow measurements, and motility experiments, parameter values  
167 for each day were calculated from fitting of the data and the reported uncertainties are  
168 from the analysis of different data sets. Normally distributed data sets were analyzed  
169 using 2-tailed student's T-tests. Data that were not normally distributed were analyzed  
170 using the non-parametric Mann-Whitney test. For the optical trapping experiments, data  
171 were analyzed using maximum likelihood estimation followed by estimation of 95%  
172 confidence intervals by 1000 rounds bootstrapping (17).

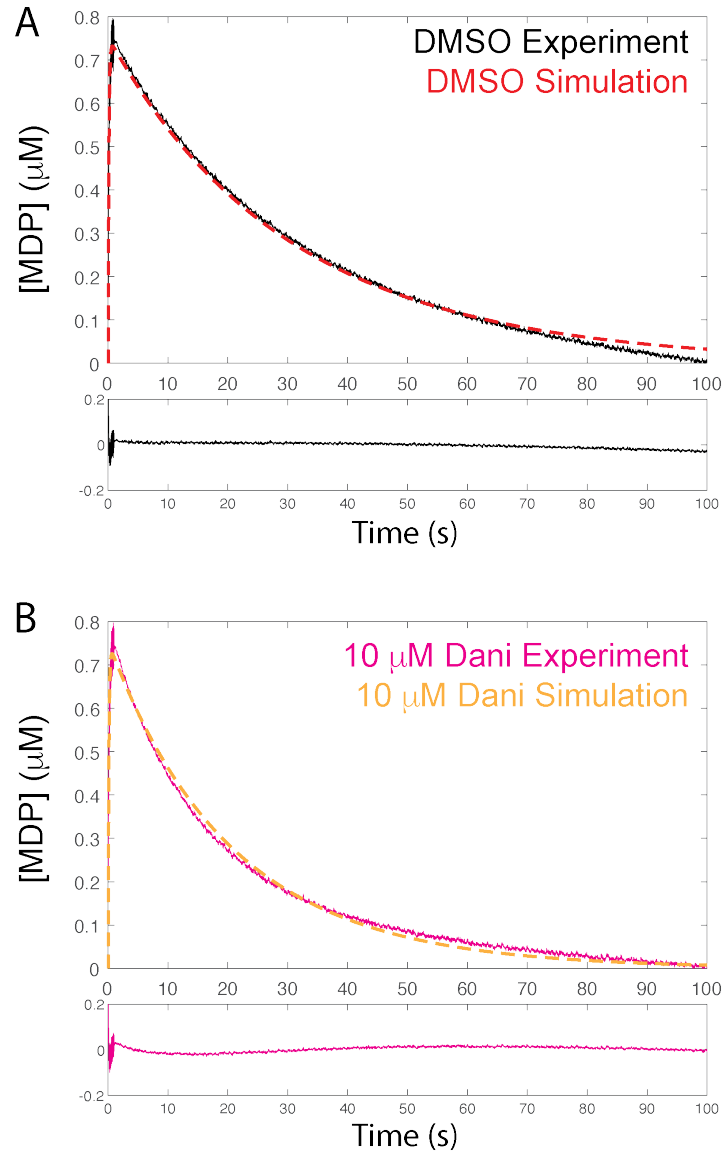


173 **Supplemental Figure 1: Single molecule optical trapping at 10  $\mu\text{M}$  ATP with**  
 174 **omecamtiv mecarbil (OM).** This is the same data as main text Fig. 3 with the addition of  
 175 a dataset collected in the presence of 10  $\mu\text{M}$  OM. The OM dataset consists of a total of  
 176 2225 single molecule binding events. Black = DMSO control. Pink = 10  $\mu\text{M}$  danicamtiv.  
 177 Orange = 10  $\mu\text{M}$  OM. **A)** Total displacements of the time forward ensemble averages. **B)**  
 178 Cumulative distributions of myosin's total working stroke size. Dotted lines are fits to a  
 179 cumulative gaussian distribution. Myosin's working stroke was  $4.9 \pm 9.7$  nm in the  
 180 absence of drugs. Danicamtiv reduced the working stroke to  $3.0 \pm 9.0$  nm. OM almost  
 181 eliminated the working stroke ( $0.7 \pm 7.1$  nm). A one-way ANOVA was used to test for  
 182 significance ( $P < 0.001$ ) and Tukey post-hoc was used for pairwise comparison. All  
 183 comparisons were significantly different ( $P < 0.001$  for each pairwise comparison). **C)**  
 184 Cumulative distribution of attachment durations. Single exponential functions were fit to  
 185 the distributions using maximum likelihood estimation. 95% confidence intervals were  
 186 calculated using bootstrapping methods. There is no statistical difference between control  
 187 and 10  $\mu\text{M}$  danicamtiv, 23 ( $-3/+3$ )  $\text{s}^{-1}$  vs. 24 ( $-1/+1$ )  $\text{s}^{-1}$  ( $P = 0.48$ ). Unlike danicamtiv, OM  
 188 slows the actomyosin detachment rate to 11 ( $-1/+1$ )  $\text{s}^{-1}$ . A Kruskal-Wallis ranks test (non-  
 189 parametric) was used to compare all groups ( $P < 0.001$ ) and Dunn's post-hoc used for

190 pairwise comparison. The control and danicamtiv conditions were both significantly  
191 different than OM ( $P < 0.001$  for those pairwise comparisons with Sidak correction).



192 **Supplemental Figure 2: Single molecule optical trapping at 1 mM ATP with and**  
 193 **without 10 μM danicamtiv.** Black = DMSO control. Pink = 10 μM danicamtiv. **A)**  
 194 Cumulative distribution of working stroke displacements. DMSO control has a larger  
 195 working stroke than myosin treated with 10 μM danicamtiv ( $5.1 \pm 6.8$  nm vs.  $2.6 \pm 7.2$  nm,  
 196  $P < 0.001$ ) at 1 mM ATP. **B)** Cumulative distribution of attachment durations. 95%  
 197 confidence intervals were calculated using bootstrapping methods. There is no different  
 198 in the detachment rate between treated and DMSO controls ( $41.4$  ( $-6.6/+6.8$ ) vs.  $34.2$  ( $-$   
 199  $5.7/+7.1$ )  $s^{-1}$ ,  $P = 0.15$ ). Note, the curves overlay. Data also reported in **Table 2** in main  
 200 text.  $N = 1755$  actomyosin binding events for the control conditions and  $N = 2107$  for 10  
 201 μM danicamtiv.

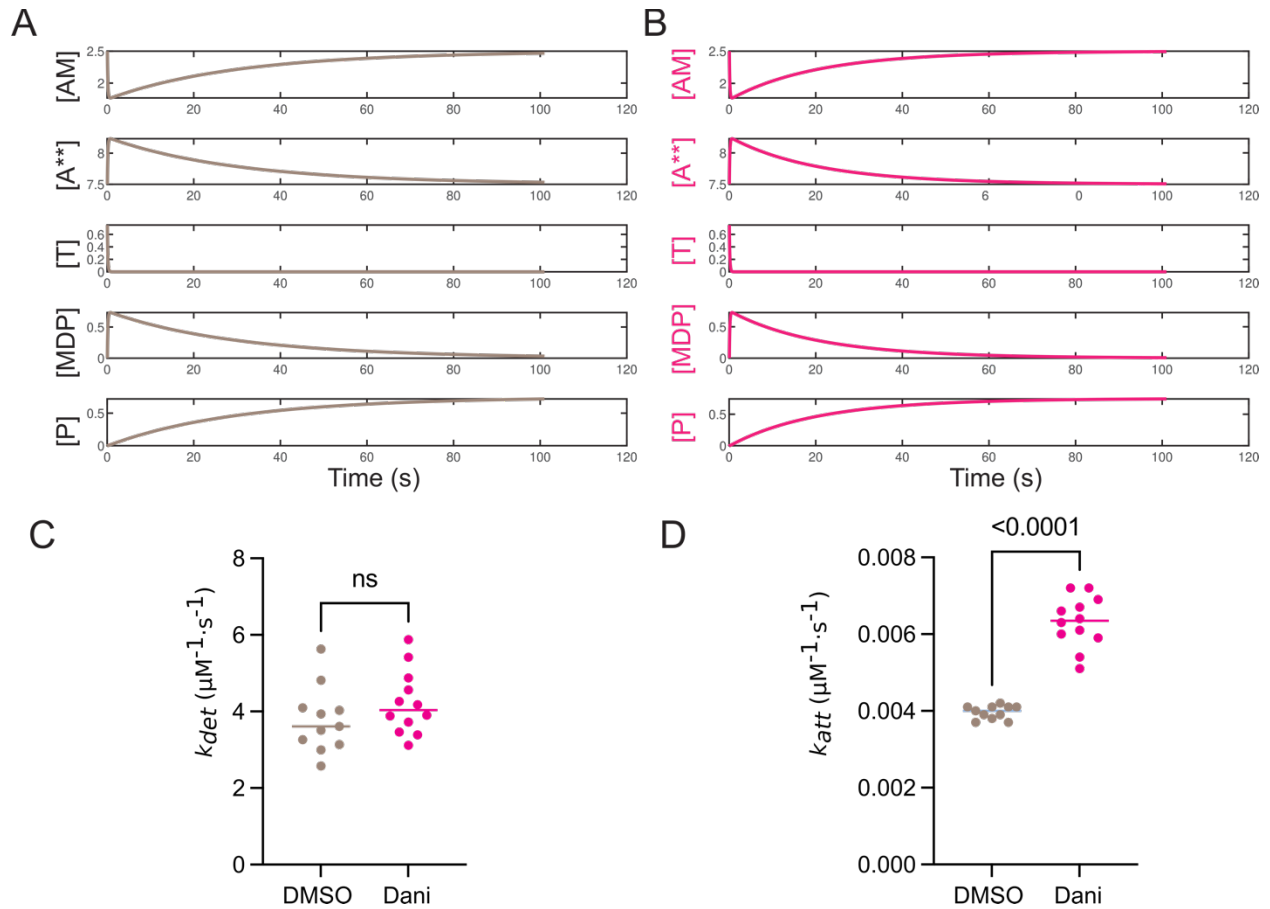


202

203 **Supplemental Fig. 3: Fitting single turnover experiments using simulations.**

204 Representative data traces are shown for **A)** DMSO control and **B)** 10  $\mu\text{M}$  danicamtiv.

205 Lower panels show residuals of the fit.



206

207 **Supplemental Figure 4: Single turnover simulations.** Calculated chemical species

208 from the best fitted parameters for **A**) DMSO and **B**) 10 μM danicamtiv. AM = actomyosin,

209 A\*\* = unbound actin, T = ATP, MDP = myosin\*ADP\*Pi, P = phosphate. Best fit parameters

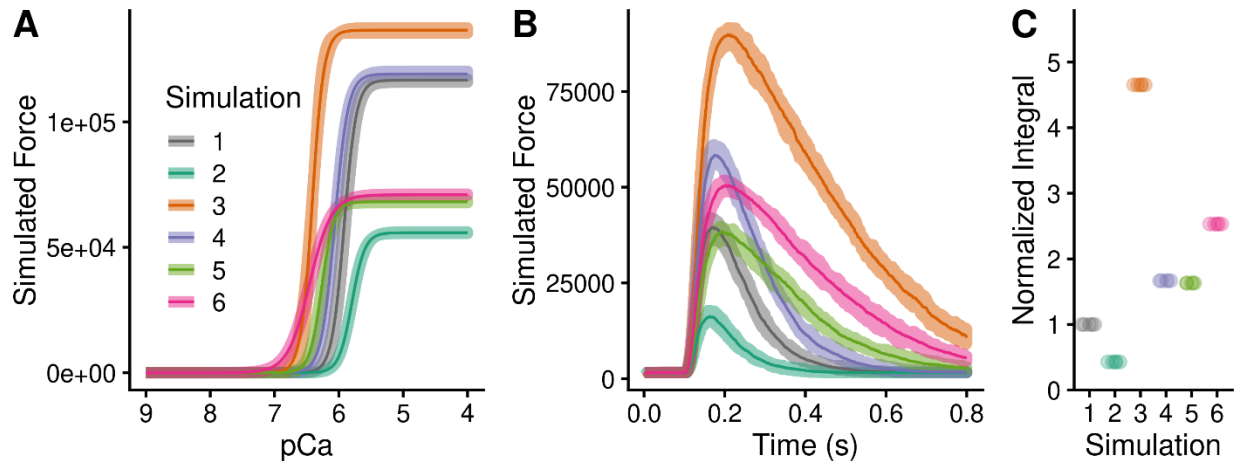
210 for the second-order rates of **C**) actomyosin detachment ( $k_{det}$ ) and **D**) subsequent

211 actomyosin attachment ( $k_{att}$ ). Data is also presented in **Fig. 5**. Each point represents a

212 single fitted transient and bars show the median. Statistical testing was done using a

213 Mann-Whitney test. Note that these are the second-order rate constants that depend on

214 the concentrations of species, not the observed rate constants.



215

216 **Supplemental Figure 5: Computational modeling of danicamtiv's effects on muscle**

217 **contraction. A) Force calcium-relationship. B) Twitch contraction in response to a**

218 **calcium transient. C) Normalized force integrals of the twitch contractions in "B". 5**

219 **replicates were conducted, the shaded region shows the range of values, and the solid**

220 **line shows the mean. The simulations show the effects of:**

221 1) Base model

222 2) Decreased working stroke (reduced by 1/2 based on optical trapping)

223 3) Increased actin attachment (increased by 2X based on single turnover  
224 measurements)

225 4) Increased population of active myosin heads (SRX → DRX) (increased by 1.5X  
226 based on x-ray diffraction data)

227 5) Decreased working stroke AND increased actin attachment

228 6) Decreased working stroke AND increased actin attachment AND increased

229 SRX→DRX

230

231 **Supplemental References**

- 232 1. S. R. Clippinger Schulte *et al.*, Single-molecule mechanics and kinetics of cardiac  
233 myosin interacting with regulated thin filaments. *Biophys J* **122**, 2544-2555 (2023).
- 234 2. S. R. Clippinger *et al.*, Disrupted mechanobiology links the molecular and cellular  
235 phenotypes in familial dilated cardiomyopathy. *Proc Natl Acad Sci U S A* **116**, 17831-  
236 17840 (2019).
- 237 3. S. S. Margossian, S. Lowey, Preparation of myosin and its subfragments from rabbit  
238 skeletal muscle. *Methods Enzymol* **85 Pt B**, 55-71 (1982).
- 239 4. J. A. Spudich, S. Watt, The regulation of rabbit skeletal muscle contraction. I.  
240 Biochemical studies of the interaction of the tropomyosin-troponin complex with  
241 actin and the proteolytic fragments of myosin. *J Biol Chem* **246**, 4866-4871 (1971).
- 242 5. S. K. Barrick, S. R. Clippinger, L. Greenberg, M. J. Greenberg, Computational Tool to  
243 Study Perturbations in Muscle Regulation and Its Application to Heart Disease.  
244 *Biophys J* **116**, 2246-2252 (2019).
- 245 6. E. M. De La Cruz, E. M. Ostap, Kinetic and equilibrium analysis of the myosin ATPase.  
246 *Methods Enzymol* **455**, 157-192 (2009).
- 247 7. J. Cubuk *et al.*, Structural dynamics of the intrinsically disordered linker region of  
248 cardiac troponin T. *bioRxiv* 10.1101/2024.05.30.596451 (2024).
- 249 8. L. Greenberg *et al.*, Harnessing molecular mechanism for precision medicine in  
250 dilated cardiomyopathy caused by a mutation in troponin T. *bioRxiv*  
251 10.1101/2024.04.05.588306 (2024).



- 252 9. S. K. Barrick, L. Greenberg, M. J. Greenberg, A troponin T variant linked with pediatric  
253 dilated cardiomyopathy reduces the coupling of thin filament activation to myosin  
254 and calcium binding. *Mol Biol Cell* **32**, 1677-1689 (2021).
- 255 10. T. Lin, M. J. Greenberg, J. R. Moore, E. M. Ostap, A hearing loss-associated myo1c  
256 mutation (R156W) decreases the myosin duty ratio and force sensitivity.  
257 *Biochemistry* **50**, 1831-1838 (2011).
- 258 11. D. M. Bers, C. W. Patton, R. Nuccitelli, A practical guide to the preparation of Ca(2+)  
259 buffers. *Methods Cell Biol* **99**, 1-26 (2010).
- 260 12. E. Meijering, O. Dzyubachyk, I. Smal, Methods for cell and particle tracking. *Methods*  
261 *Enzymol* **504**, 183-200 (2012).
- 262 13. J. Schindelin *et al.*, Fiji: an open-source platform for biological-image analysis. *Nat*  
263 *Methods* **9**, 676-682 (2012).
- 264 14. T. Blackwell, W. T. Stump, S. R. Clippinger, M. J. Greenberg, Computational Tool for  
265 Ensemble Averaging of Single-Molecule Data. *Biophys J* **120**, 10-20 (2021).
- 266 15. M. J. Greenberg, H. Shuman, E. M. Ostap, Measuring the Kinetic and Mechanical  
267 Properties of Non-processive Myosins Using Optical Tweezers. *Methods Mol Biol*  
268 **1486**, 483-509 (2017).
- 269 16. L. K. Gunther *et al.*, Converter domain mutations in myosin alter structural kinetics  
270 and motor function. *J Biol Chem* **294**, 1554-1567 (2019).
- 271 17. M. S. Woody, J. H. Lewis, M. J. Greenberg, Y. E. Goldman, E. M. Ostap, MEMLET: An  
272 Easy-to-Use Tool for Data Fitting and Model Comparison Using Maximum-Likelihood  
273 Estimation. *Biophys J* **111**, 273-282 (2016).

- 274 18. S. Kosta, D. Colli, Q. Ye, K. S. Campbell, FiberSim: A flexible open-source model of  
275 myofilament-level contraction. *Biophys J* **121**, 175-182 (2022).  
276